Highly sensitive and label-free detection of biotin using a liquid crystal-based optofluidic biosensor

HAONAN WANG,[1] TIANHUA XU,[1,2,*] ZIYIHUI WANG,[1,3] YIZE LIU,[1] HUAIXU CHEN,[1] JUNFENG JIANG,[1,4] AND TIEGEN LIU[1]

[1] *School of Precision Instrument and Opto-Electronics Engineering, Tianjin University, Tianjin, 300072, China*
[2] *School of Engineering, University of Warwick, Coventry, CV4 7AL, United Kingdom*
[3] *School of Electrical and Electronics Engineering, Nanyang Technological University, Singapore 639798, Singapore*
[4] *jiangjfjxu@tju.edu.cn*
[*] *tianhua.xu@ieee.org*

Abstract: A liquid crystal (LC)-based optofluidic whispering gallery mode (WGM) resonator has been applied as a biosensor to detect biotin. Immobilized streptavidin (SA) act as protein molecules and specifically bind to biotin through strong non-covalent interaction, which can interfere with the orientation of LCs by decreasing the vertical anchoring force of the alignment layer in which the WGM spectral wavelength shift is monitored as a sensing parameter. Due to the double magnification of the LC molecular orientation transition and the resonance of the WGM, the detection limit for SA can reach 1.25 fM (4.7×10^{-13} g/ml). The measurable concentration of biotin and the wavelength shift of the WGM spectrum have an excellent linearity in the range of 0 to 0.1 pg/ml, which can achieve ultra-low detection limit (0.4 fM), i.e., seven orders of magnitude improvement over conventional polarized optical microscope (POM) method. The proposed optofluidic biosensor is highly reproducible and can be used as an ultrasensitive real-time monitoring biosensor, which will open the door for applications to other receptor and ligand models.

1. Introduction

Biotin is a water-soluble B vitamin otherwise known as vitamin B7 (VB7) and vitamin H (VH). Biotin is a vital nutrient for mammals since it is required for the synthesis of vitamin C (VC), the maintenance of normal growth and development in the human body, and the proper metabolism of fat and protein [1,2]. However, humans and other animals cannot synthesize biotin and the biotin has to be obtained exogenously from food via the intestinal absorption or has to be procuded endogenously via coliform bacteria. As a result, infant formula must be fortified with biotin [3]. Currently available techniques for detecting biotin include microbiological tests [4], high performance liquid chromatography [5], fluorescence assays [6], and enzyme-linked immunosorbent assays [7]. These approaches, however, have a number of disadvantages, including the complicated operation, the long detection time, and the low sensitivity. As a result, the development of a rapid and highly sensitive biotin detection platform is required and critical.

Meanwhile, streptavidin (SA) is a tetrameric protein secreted by streptomyces. Similar to avidin, SA can bind to biotin molecules with high specificity through non-covalent interactions. This effect is the strongest non-covalent effect known so far, which is similar to the covalent binding strength and has a strong affinity [8,9].

Liquid crystals (LCs) can provide very sensitive biomolecule detection due to their molecular orientation-dependent behaviors to surface biomolecular binding processes. Biosensors that

utilize the LC amplification primarily rely on the birefringence features of LC molecules in combination with polarized light to detect target molecules [10–13]. The specific performance is that LC molecules will change the homeotropic alignment due to the appearance of the target biomolecules, which will lead to the transformation of the optical signal under the POM [14,15]. However, this method, which relies on the naked eye inspection, severely restricts the detection sensitivity. Due to the exceptionally high Q factor, small mode volume, and ability to significantly enhance the interaction between the light field and the matter in the cavity, WGM microcavities have obtained significant research attention in recent years [16–18]. With the confirmed feasibility of LC-based optofluidic biosensor in detection (via continuously monitoring the WGM spectrum), and the optical design of the WGM based biosensor has employed the micro-resonator structure to enhance the ability of light-matter interactions. The WGM micro-resonator made of silica has the advantages of high sensitivity, low price, and stable structure. Molecular binding events at the interface and external stimuli can trigger the orientation transition of LC molecules, and the shift in the resonant wavelength arises from the change in the effective refractive index within the WGM cavity. Compared with the conventional POM method by observing the change in LC orientation with the naked eye, the spectrum of the WGM microcavity can be excited and monitored with stronger merits. In the field of biochemical sensors, numerous benefits of the WGM method have led to its widespread applications [19,20].

In this study, we demonstrate a sensitive LC-based optofluidic resonator and explored its application for the detection of biotin. After modifying the microcavity with DMOAP, specific concentration of SA was detected, and then various concentrations of biotin were injected into the microcavity under the same concentration of SA to enable the detection of biotin molecules. The sensing parameter was captured via monitoring the WGM spectral wavelength shift. Due to the strong force generated by the combination of SA and biotin, the dual effects of LC orientation change and the resonance of the resonant cavity trigger the shift of the WGM spectrum. A higher concentration of biotin will induce a more dramatic transition in the orientation of the LC molecules, magnifying the optical signal and enhancing detection sensitivity. In this novel and exhaustive approach, biological targets can be detected by monitoring the WGM spectra of resonant cavities, seven orders of magnitude higher than POM methods with naked-eye.

2. Materials and methods

2.1. Materials

The silica capillary used to fabricate the microcavity was purchased from Polymicro Inc. (#TSP250350). The 4-Cyano-4′-N-Pentylbiphenyl as nematic LC (5CB) and Dimethyloctadecyl [3-(trimethoxysilyl)propyl] ammoniumchloride (DMOAP, #A-FF032) to modify the internal surface of the microbubble were obtained from Xianding Biotechnology Co., Ltd. (Shanghai, China). Streptavidin (SA) (#S9171), biotin (#SB8530) and goat anti-human IgG (AHIgG) (#PA101) were purchased from Solarbio Science & Technology, Co., Ltd. (Beijing, China). Human IgG (HIgG) (#bs-0297P) and human cardiac troponin (CTnI) (#bs-41212P) was purchased from Bioss Biotechnology Co., Ltd. (Beijing, China). Cobalamin (vitamin B12) (#WSS-B12 from Tianjin Shengbaihao Biotechnology Co., Ltd., Tianjin, China), folic acid (vitamin B9) (#A57624 from Innochem, Beijing, China) and pyridoxine (vitamin B6) (#65-23-6 from Heowns, Tianjin, China) were used for the specific detection. Infant formula used for real sample detection was purchased from Feihe Dairy Co., Ltd. (Heilongjiang, China).

2.2. Preparation of microbubble and tapered fiber

In this study, the hollow microcavity is employed in the WGM optofluidic biosensor. Due to the surface tension of silica capillary, WGM microcavity with the shape of microbubble can be created by heating and pressing. The silica capillary was first heated and stretched using

a centimeter-diameter hydrogen-oxygen flame. A digital microscope was used to observe the expansion process after switching to a tiny fire with a millimeter-diameter fire flame and the barometric pressure was continuously injected into the silica capillary. By adjusting the stretching length, flame size, and additional pressure during the expansion process, the diameter and the wall thickness of the microbubble chamber could be changed. In this study, microbubble of 190 μm in diameter and 2-3 μm in wall thickness was produced. To keep the microbubble from being damaged, UV adhesive is used to attach both ends of the microbubble to the copper tablet. The microcavity is coupled via tapered fiber. Tapered fiber with diameter of 1-2 μm can also be produced using the flame-heated stretching technique [21].

2.3.　Decoration of the inner surface with DMOAP and biomolecules

DMOAP at a concentration of 1 % (v/v) was injected into the microbubble at a flow rate of 0.7 μL/min for 30 min using a syringe pump. The excess DMOAP solution was then rinsed with deionized water for 1 min. The configured SA with 10^{-3} g/mL concentration was filled into the microbubble for 1 h. Then the deionized water was used to remove excess protein molecules, followed by different concentrations of biotin injected for 1 h for the detection of biotin. LCs then injected into the microbubble with the same pumping setup. The syringe pump (#SPLab01 from Shenchen Precision Pump Co., Ltd., Baoding, China) was used to inject reagents into microcavity.

2.4.　Preparation of a LC optofluidic biosensor for SA and biotin detection

At one end of the microbubble, the syringe with LCs was connected to the silica capillary. LC molecules were gradually fed into the modified microbubble at a pace of 0.7 μL/min by a pump to avoid the signal instability due to the over fast injection of the LCs. By examining the microscopical image and the laser spectrum, it is possible to determine whether LCs have been loaded into the microbubble. A grooming light field surrounds the microbubble on the microscopic image, and the spectrum appears denser. Simultaneously, the capillary at the other end of the microbubble was sealed with the UV glue in order to ensure the stable air pressure in the cavity and to prevent the flow motion of LCs. The automated pump was then switched off and the data was recorded.

2.5.　Optical setup

Polarized images were captured by a polarized light microscope (XP-203E, Changfang, Shanghai, China). The input laser beam was generated, for the WGM sensing system, using a tunable laser (Keysight 81607A, linewidth < 10 kHz) with a wavelength range of 1560 nm to 1580 nm. The laser beam was then fed into the LC-based optofluidic microcavity through a fiber taper in order to produce the WGM spectrum, which was then detected by the optical power meter (Keysight 81636B) connected to the PC.

3.　Results and discussions

3.1.　Effect of he microbubble diameter on the spectral response of an LC-based optofluidic biosensor

In order to obtain intuitive detection results, we have investigated the polarization mode of the WGM microcavity. For the homeotropic orientation of LCs without biomolecules added, the TM polarization in which the electric field oscillates perpendicularly to the microcavity surface experiences a higher permittivity along the long axis of the LC molecules, corresponding to the extraordinary refractive index ($n_e = 1.67$) [22]. In contrast, with the addition of biotargets, the orientation of the LC molecules tends to become planar, with the TM polarization corresponding to the ordinary refractive index ($n_o = 1.51$). In accordance with the change in the orientation of

the LC molecules, the WGM spectral response varies with the LC refractive index from n_e to n_o [23,24], and a blue-shift phenomenon of the spectrum is observed.

A few microbubble resonators have been fabricated with diameters ranging from 190 μm to 260 μm at an interval of 15 μm (190 μm, 205 μm, 230 μm, 245 μm, 260 μm) in order to detect the output WGM spectra. During the process of the preparation, parameters of the fire flame and the stretching length are managed to ensure the comparable wall thickness of each microbubble cavity. The free spectral range (*FSR*) and the optical modes of the WGM microcavity is depicted in Fig. 1(a) as a characteristic parameter to describe this biosensor platform (190 μm). Fig. S1 illustrates the size dependence of WGM resonators by comparing the spectra of microbubbles with different diameters. The *FSR* is an important parameter for WGM resonators. Results indicate that the *FSR* is dependent on the size of the micro-resonator, and is proportional to the reciprocal of the diameter (1/*D*) of the resonator [25,26]. As the diameter of the microcavity decreases, the *FSR* value increases, as seen in Fig. 1(b), which satisfies the relationship *FSR* ~ 1/*D*.

$$FSR = \frac{\lambda_n^2}{\pi D n_{eff}} \tag{1}$$

where n_{eff} is the effective refractive index determined by the external environment and the microcavity material, and *D* is the diameter of the microbubble.
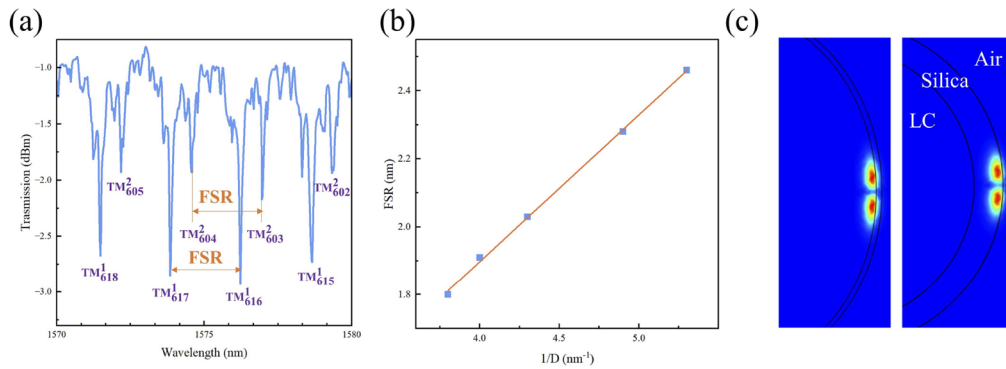

Fig. 1. (a) WGM spectra of LC-based WGM resonator from which the *FSR* can be estimated to be 2.46 nm and the optical modes of WGM spectrum fitted to first order (*q* = 1) TM modes from 615-618, and the second order (*q* = 2) TM modes from 602-605. (b) Relationship between FSR and 1/*D* of the WGM micro-resonator. The FSR is proportional to the reciprocal of the diameter (1/*D*) of resonator. The orange line represents the linear fitting curve. (c) Electric field distribution for microcavity with wall thicknesses of 2 μm and 10 μm respectively.

In addition, the number of the WGM lasing modes in the LC-based optofluidic micro-resonator can be calculated by following equation [24]:

$$\lambda^{-1}(R, n_1, n_r, q, m) = \frac{1}{2\pi n n_1}\left[m + \frac{1}{2} + 2^{-\frac{1}{3}}\alpha(q)\left(m + \frac{1}{2}\right)^{\frac{1}{3}} - \frac{L}{(n_r^2 - 1)^{\frac{1}{2}}} + \frac{3}{10}2^{-\frac{2}{3}}\alpha^2(q)\left(m + \frac{1}{2}\right)^{\frac{1}{3}} - 2^{-\frac{1}{3}L}\left(n_r^2 - \frac{2}{3}L^2\right)\frac{\alpha(q)\left(m + \frac{1}{2}\right)^{\frac{2}{3}}}{(n_r^2 - 1)^{\frac{3}{2}}} \right] \tag{2}$$

where *R* is the micro-resonator radius, $n_r = \frac{n_1}{n_2}$, $\alpha(q)$ is the roots of the Airy function [27]. $L = \frac{1}{n_r}$ for the transverse magnetic (TM) mode and $L = n_r$ for the transverse electric (TE) mode. The *R* of the proposed micro-resonator is 190 μm, refractive index n_1=1.44 and n_2= 1.67 for the silica and extraordinary refractive index of LC. Theoretical calculation indicates that the WGM spectrum fitted to the first-order (*q* = 1) TM modes from 615-618, and the second-order (*q* = 2) TM modes from 602-605.

To increase the detectable range of the micro-resonator, it is necessary to control the size of the microcavity in experiment. When the *FSR* of the microcavity becomes larger, the response of the microcavity sensor to an external signal can also be enhanced. The wavelength or the frequency interval of WGM resonance peaks in adjacent longitudinal modes is extremely stable, hence the *FSR* is an essential criterion for determining if the optical mode of the microcavity conforms to the WGM. At the same time, since the energy of the evanescent field decreases exponentially with the depth of penetration into the medium, the selection of microcavity diameter and wall thickness is very important. The microcavity prepared by inflating and pressurizing the inside of the silica capillary has a thicker wall thickness when the diameter is smaller [28,29]. A thin microcavity wall thickness results in more WGMs being distributed inside the cavity, as shown in the Fig. 1(c). When the wall thickness is greater than 10 μm, the WGM field distribution only propagates along the silica region, and the interaction between light and biomolecules and the orientation transition of LC cannot be monitored. In addition, LC molecules on the surface can transmit variations in their orientations within a proximity (maximum 100 μm) to amplify the sensing signal [30]. Therefore, in order to ensure a thin wall thickness and comprehensively monitor the orientation changes of LC molecules, a microbubble cavity with a diameter of 190 μm was finally selected.

3.2. LC-based optofluidic biosensor for SA detection

Based on LC and micron-scale WGM microcavity, a passive resonant cavity is designed, and an optofluidic sensor amplified by LC is developed. The supersensitive monitoring of protein molecules and small biomolecules at femtomole level is realized through the orientation transformation of LC molecules. The incident laser emitted from a tunable continuous-wave (CW) laser (as the pump source, from 1560-1580 nm) is transmitted efficiently through the tapered fiber, exciting the WGM mode in the cavity by coupling the evanescent field with the microcavity and then observed by the microscope with a charge coupled device camera, the sensing platform is shown in the Fig. 2(a). With the addition of SA, the induced layer of LC molecular orientation formed on the inner surface of the microcavity by the injected DMOAP solution (which orientates LCs homeotropically) will be disturbed by biomolecules, reducing the vertical force on the LC molecules. Using a tunable bracket, a precise adjustment can be achieved to control the distance between the tapered fiber and the microbubble cavity, as shown in Fig. 2(b), in order to achieve the phase matching and the evanescent field coupling. The interplay of light and analyte also happens on the inner surface of the microcavity. At this point, LC molecules will be aligned horizontally.

At 10^{-3} g/ml SA, the maximum signal response reaches 2.2 nm and the spectral changes are shown in Fig. 3(a). The total wavelength shift of the spectral response behaves linearly over the concentration ranges from 10^{-9} g/ml to 10^{-12} g/ml (Fig. 3(b)). On the basis of the fitted curve, it is determined that the limit of detection (LOD) is 1.25 fM (4.7×10^{-13} g/ml). At concentrations below 10^{-6} g/ml, the POM detection method can no longer detect the the concentration of SA. Therefore, the WGM spectral shift caused by the orientation change of the LC in the microcavity enables the protein concentration sensing, and this simple, high-sensitivity, and compact protein assay detection platform provides a new promising and feasible solution for biosensing applications.

3.3. LC-based optofluidic biosensor for biotin detection

A well-known receptor-ligand model, biotin–avidin binding is used to amplify and transduce receptor-mediated binding. With an affinity constant of 10^{15} L/mol, the non-covalent SA-biotin binding provides a general bridge for many diverse applications which are commonly used to detect and monitor specific biological targets due to the exceptionally strong binding affinity [31].
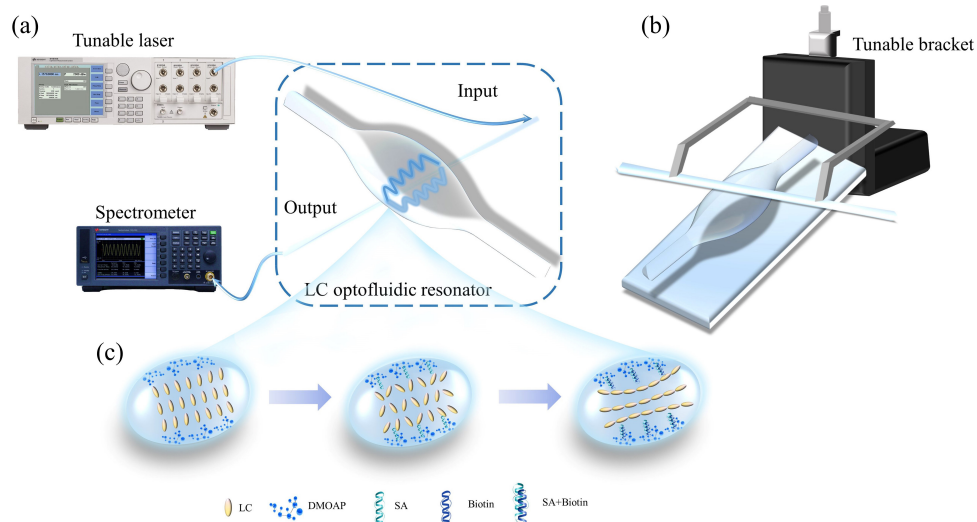
Fig. 2. Schematic of the (a) LC-based optofluidic sensing experimental platform. The WGM spectrum was acquired by coupling light from a tunable laser into an LC-amplified optofluidic resonator through a fiber taper and then observing it with the computer connected to the optical power meter. (b) The distance between the tapered fiber and the WGM microcavity is adjusted by the displacement stage. (c) Illustration of the LC-based optofluidic biosensor for biotin detection. The homeotropic orientation of LC molecules induced by DMOAP is disturbed due to the presence of SA and the specific binding of SA to biotin.
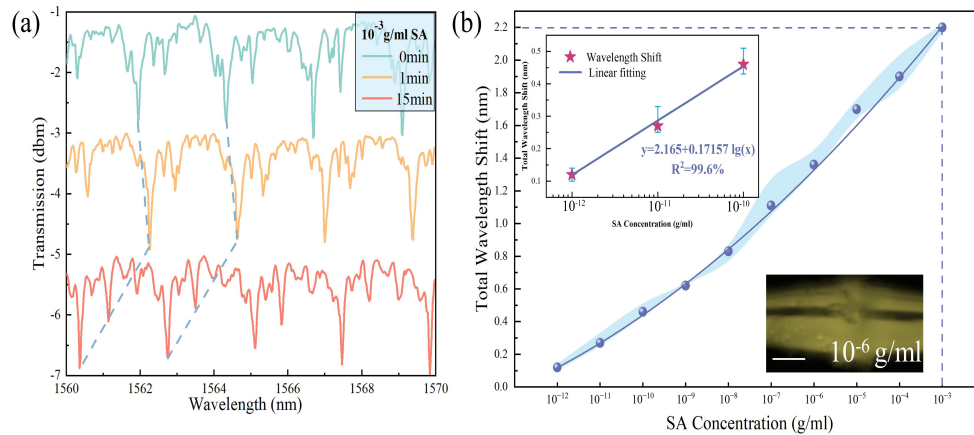

Fig. 3. (a) Spectral response of SA at 10^{-3} g/ml concentration. (b) The total wavelength shift at different concentrations of SA (10^{-3} g/ml to 10^{-12} g/ml). The total spectral shift equals the addition of the absolute values of the red and blue spectral shifts. Inset: the linear relationship curve between the concentration of 10^{-10} g/ml and the concentration of 10^{-12} g/ml and the POM image of the concentration of 10^{-6} g/ml cannot be distinguished by naked eyes at this time. Scale bar: 100 μm.

After immobilizing DMOAP and a constant concentration of SA (10^{-3} g/ml) on the internal surface of the micro-resonator, various concentrations of biotin solutions were added for detection. It is anticipated that biotin would bind to SA, and can thereby weaken the vertical anchoring force of DMOAP on LC molecules, to increase the amount of spectral shift. The arrangement direction of LC molecules is relatively disordered when the nematic LC (5CB) stays alone. By observing POM images of the LC microcavity, the rule of the change in the LC orientation during the biotin detection is obtained. The characteristics of the polarized light are used to examine the alignment of LC molecules in the microbubble. Throughout the experiment, both DMOAP and biotin are adhered to the inner surface of the microbubble. As a result of the interaction between biological and LC molecules, the theoretical orientation of LC molecules is shown in Fig. 2(c). It is observed that when LC molecules are aligned homeotropically due to the DMOAP coating, the polarized light cannot pass through the microbubble. The dark background in the middle of the microbubble is attributed to the homeotropic alignment of LC molecules [32]. The infusion of biotin changes the center of the microbubble into a bright polarized optical image. Different concentrations of biotin correspond to different POM images of LCs observed by the naked eye were obtained after 15 mins, as shown in Fig. S2. According to POM images of biotin at high concentrations, the self-assembled configuration of LCs was modified, and the biotin molecules resulted in LC molecules being rearrangement [33]. However, for low concentrations of biomolecules (less than 10^{-7} g/ml), it is difficult to detect small changes in LCs through POM, and the detection sensitivity is inadequate. Consequently, it is demonstrated that the strong non-covalent interaction between SA and biotin molecules can change the alignment of LC molecules.

Although the POM detection method can handily reflect the approximate concentration range, it cannot quantitatively and precisely obtain the specific concentration of biotin. It relies mostly on the naked eye inspection, which is incapable of quantitatively analyzing the variation of the internal response of the microbubble and suffers from the low sensitivity, which hinders the development of LC-based biosensors. Correspondingly, our optofluidic biosensor has high sensitivity and is an effective way to replace naked eye detection.

According to our previous study, the injection of LC into the micro-resonator using a syringe pump at a low flow rate (0.7 μL/min) can assure sufficient intermolecular reflection and increase the sensitivity of the LC-based biomolecule detection. WGM spectral data recording began from 15 seconds after the LCs reached the optofluidic resonator and ended at 15 mins after the start, in order to avoid the measurement instability caused by an excessively rapid spectral shift at the beginning and to prevent halting the experiment before the completion of the spectral shift. Fig. S3 illustrates the stability of the optofluidic biosensor in the absence of biomolecules (with DMOAP and LCs only), where there is a minimal spectral wavelength shift, caused by the laser instability. The spectral curves of biotin concentrations of 10^{-10} g/ml and 10^{-5} g/ml at 0 min, 1 min and 15 mins are shown in Fig. 4(a) and Fig. 4(b), and a significant spectral shift can be observed. The WGM spectral response demonstrates a redshift tendency first followed by a blueshift trend. The redshift deviation is registered as the value of positive number, while the blueshift deviation is recorded as the value of negative number. The total wavelength shift refers to the sum of the absolute values of the redshift and the blueshift. The red shift occurs due to the absorption behavior of biomolecules. The interaction between the evanescent field formed on the outer surface of the microcavity and the biomolecules polarizes the molecules, leading the shift of the photon energy of the resonant state, and changes the frequency of the resonant wavelength [34]. Therefore, the wavelength response in the transmission spectrum comes from the combined action of the interfacial adsorption of biomolecules and the orientational transition of LCs. The real-time monitoring spectra at concentrations of 10^{-3} g/ml to 10^{-13} g/ml are shown in the Fig. 4(c). To demonstrate the repeatability of the biosensing platform, the same micro-resonator was utilized in three consecutive experiments with different concentrations of

10^{-3} g/ml, 10^{-8} g/ml and 10^{-13} g/ml, ensuring a highly repeatable and stable spectral signal response performance of the sensing platform (Fig. S4).
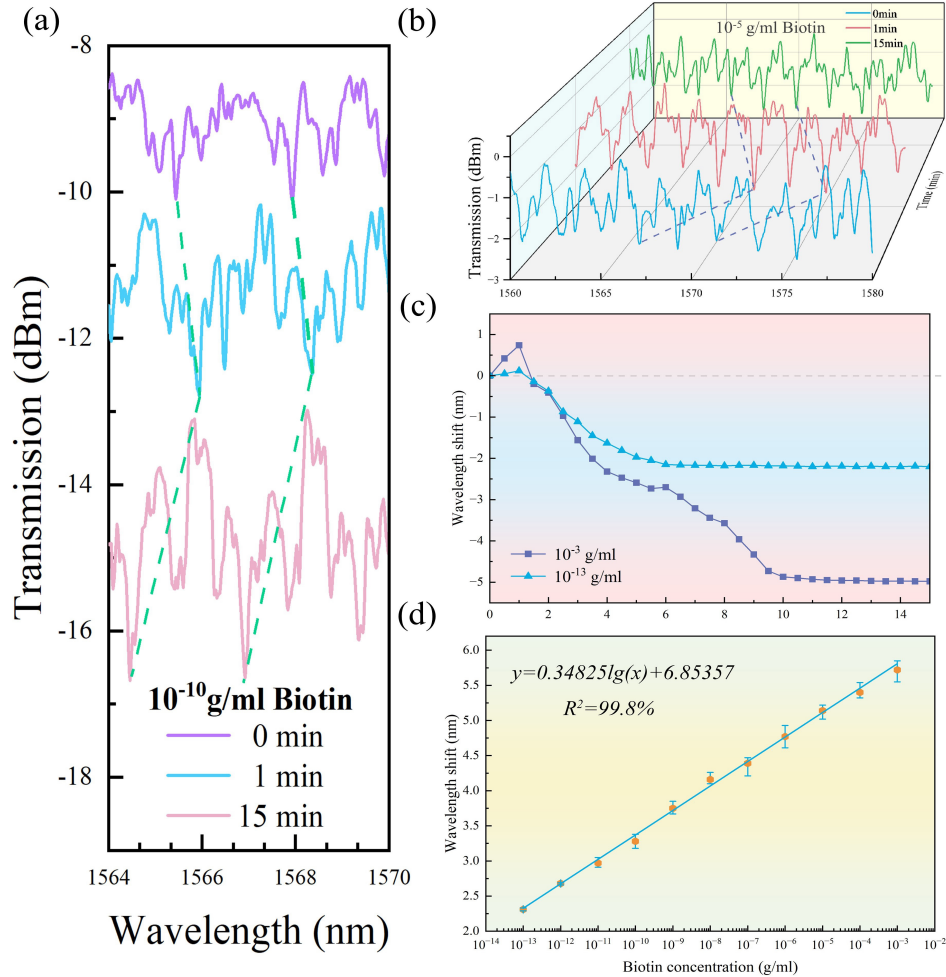

Fig. 4. (a) WGM spectral shift at a biotin concentration of 10^{-10} g/ml. (b) WGM lasing spectra of LC-based optofluidic micro-resonator recorded after 15 min of 10^{-5} g/ml biotin addition. (c) WGM laser spectrum shift of the LC-based optofluidic micro-resonator under the highest and lowest (10^{-3} g/ml and 10^{-13} g/ml.) biotin concentrations be monitored in real-time within 15 mins. (d)The overall wavelength shift responses under different concentrations of biotin (10^{-3} g/ml to 10^{-13} g/ml). The spectral shift has a linear relationship with the concentration of biotin.

A significant improvement in wavelength shift was observed when biotin was added at different concentrations in comparison to SA alone. Based on section 3.2, the sum of the wavelength shift at the concentration of 10^{-3} g/ml SA is about 2.2 nm. The total wavelength shift of WGM spectra with respect to different concentrations of biotin was recorded as shown in Fig. 4(d). It is shown that the combination of biotin and SA increased the total distance of WGM spectral shift. At a fixed SA concentration, the total shift experienced by the spectral increase becomes larger as the biotin concentration increases. Therefore, we can speculate that the strong non-covalent force generated by the combination of biotin and SA can drastically disturb the alignment of LC and promote the interaction between biomolecules and LC molecules. As a consequence,

it could theoretically be used to make a more sensitive biomolecular sensor. Based on the curve-fitting, the detection limit of our LC-based WGM optofluidic platform is approximately 0.4 fM (9×10^{-14} g/ml), which is compared with other methods for biotin detection illustrated in Table S1. Consequently, it can be demonstrated that the specific binding created by the addition of biotin can induce the alignment transition of LC molecules. There is a more pronounced spectral shift due to the specific binding of SA-biotin upon addition of biotin. Therefore, further combination of nanoparticle amplification is expected to develop biotin sensors with higher specificity and sensitivity [35,36].

In addition, to verify the feasibility of the sensor for sensing other proteins and specifically bound ligands and receptor models, human immunoglobulin (HIgG) and human cardiac troponin (CTnI) were tested (Figure S5), and the detection limits were 1.3×10^{-10} g/ml and 1.09×10^{-10} g/ml, respectively. The results show that the optofluidic sensor has universal detection of protein molecules and high sensitivity. At the same time, 1 mg/ml HIgG and different concentrations of goat anti-human immunoglobulin (goat AHIgG) were used as receptor and ligand models to detect goat AHIgG. For specific binding events, the wavelength shift of WGM spectrum can reach 4.14 nm, and the detection limit of goat AHIgG is lower, demonstrating the high specificity of the sensor. The proposed LC-based WGM optofluidic sensor can be used as a cost-effective tool for early disease diagnosis.

3.4. Selectivity of a LC-based optofluidic biosensor for biotin detection

The optofluidic sensing platform based on LC amplification is designed on the basis of the non-covalent binding of biotin to SA. In order to illustrate the specific selectivity of the sensor, various B vitamins, including pyridoxine (vitamin B6), folic acid (vitamin B9), and cobalamin (vitamin B12), have been applied as the specific identification capacity substance. The concentration of all chemicals were determined to be 10^{-3} g/ml, and microbubble with the same diameter and wall thickness was utilized. The spectrum shifted dramatically only in the presence of biotin, whereas the spectrum shifted similarly in the presence of SA and the control group. This result demonstrated that B6, B9 and B12 are incapable of triggering a large change in the alignment of LC molecules and thus cannot lead to a significant wavelength shift, as displayed in Fig. 5. The selectivity of LC-based optofluidic sensors to detect biotin may be a result of the high-affinity binding of SA-biotin and the following competition produced by the binding event.
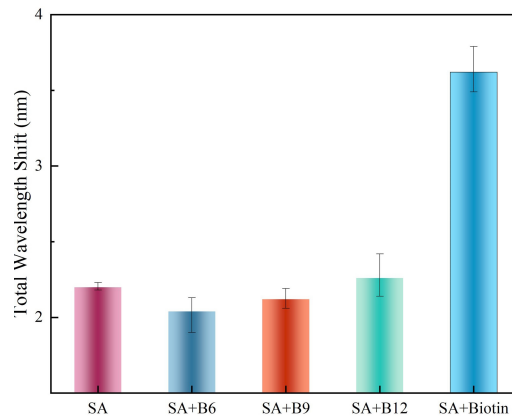

Fig. 5. WGM spectral response of LC-based optofluidic biosensor to different substances (B6, B9, B12). All the compounds are 10^{-3} g/ml.

4.   Detection of biotin in real samples

To further determine the practical applicability of the LC-based optofluidic sensing platform to real samples, infant formula purchased from local supermarket have been applied in experiment. The formula milk powder with known biotin content was selected as the matrix, and biotin standards of different concentrations were added to carry out the recovery rate experiment. The purchased infant formula is known to contain 16 μg of biotin per 100 g. A solution with a concentration of 16 ng/ml was prepared from milk powder by high temperature inactivation of protein and centrifugation. As shown in Table 1, biotin with concentrations of 10, 100, 200, 500 ng/ml were added into the diluted formula milk separately. Recovery rates of 93.5% for 10 ng/ml, 98.8% for 100 ng/ml, 103.7% for 200 ng/ml, and 104% for 500 ng/ml have been achieved, respectively. This demonstrates that the performance of the optofluidic sensor is quite accurate and reproducible, and can be applied to the practical sample detection.

Table 1. Recovery experiments of determination of biotin in infant formula samples

Biotin addition (ng/ml)	Measured amount (ng/ml)	Recovery rate (%)
0	16	-
10	25.35	93.5
100	114.79	98.8
200	223.47	103.7
500	535.92	104.0

5.   Conclusions

In this study, we developed a highly sensitive optofluidic resonator that employs LC amplification for quantitative analyses of biotin and SA. Biotargets immobilized in the modified WGM micro-resonator trigger an orientational transition of LC molecules, which can be amplified and used to assess the concentration of target molecules via wavelength changes. It is found that the overall WGM spectral shift is proportional to concentrations of the biotin and the SA and the detection limit can reach as low as the femtomole-level. It is also verified that this developed biosensor exhibits good selectivity for the biotin detection due to the high specificity and the strong non-covalent binding between SA and biotin. Our LC-based optofluidic WGM biosensor is capable of detecting various types of protein molecules and models of other receptor-ligand binding, which provides a high-sensitivity, fast-response and low-cost solution for the ultrasensitive label-free protein detection.

Disclosures. The authors declare there are no conflicts of interest.

Data availability. Data underlying the results presented in this paper are not publicly available at this time but may be obtained from the authors upon reasonable request.

Supplemental document. See Supplement 1 for supporting content.

References

1. W.-Z. Lin, W.-C. Liao, F.-H. Chen, I.-C. Ma, and S.-Y. Hou, "Detection of biotin with zeptomole sensitivity using recombinant spores and a competition assay," Anal. Bioanal. Chem. **412**(26), 7219–7226 (2020).
2. O. Livnah, E. A. Bayer, M. Wilchek, and J. L. Sussman, "Three-dimensional structures of avidin and the avidin-biotin complex," Proc. Natl. Acad. Sci. U.S.A. **90**(11), 5076–5080 (1993).
3. H. E. Indyk, E. A. Evans, M. C. B. Caselunghe, B. S. Persson, P. M. Finglas, D. C. Woollard, and E. L. Filonzi, "Determination of biotin and folate in infant formula and milk by optical biosensor-based immunoassay," J. AOAC Int. **83**(5), 1141–1148 (2000).

4. T. Tsukatani, H. Suenaga, M. Ishiyama, T. Ezoe, and K. Matsumoto, "Determination of water-soluble vitamins using a colorimetric microbial viability assay based on the reduction of water-soluble tetrazolium salts," Food chemistry **127**(2), 711–715 (2011).

5. H. Chen, Y. Feng, Y. Cao, Y. Tang, and T. Liu, "A study on the detection of free and bound biotin based on tr-fret technology," Analyst **147**(2), 318–324 (2022).

6. H. Zhang, Y. Li, and X. Su, "A small-molecule-linked DNA–graphene oxide-based fluorescence-sensing system for detection of biotin," Analytical biochemistry **442**(2), 172–177 (2013).

7. S. M. Sedlak, L. C. Schendel, H. E. Gaub, and R. C. Bernardi, "Streptavidin/biotin: tethering geometry defines unbinding mechanics," Sci. Adv. **6**(13), eaay5999 (2020).

8. S. A. Lincy, Y. A. Richard, T. Vinitha, K. Balamurugan, and V. Dharuman, "Streptavidin Fe_2O_3-gold nanoparticles functionalized theranostic liposome for antibiotic resistant bacteria and biotin sensing," Biosensors and Bioelectronics **219**, 114849 (2023).

9. D. Zhao, Y. Peng, L. Xu, W. Zhou, Q. Wang, and L. Guo, "Liquid-crystal biosensor based on nickel-nanosphere-induced homeotropic alignment for the amplified detection of thrombin," ACS Appl. Mater. Interfaces **7**(42), 23418–23422 (2015).

10. S. Lu, Y. Guo, L. Qi, Q. Hu, and L. Yu, "Highly sensitive and label-free detection of catalase by a H_2O_2-responsive liquid crystal sensing platform," Sensors and Actuators B: Chemical **344**, 130279 (2021).

11. T.-K. Chang, M.-J. Lee, and W. Lee, "Signal amplification strategies for optical biodetection at the liquid crystal–solid interface," Liq. Cryst. pp. 1–11 (2023).

12. T.-K. Chang, M.-J. Lee, and W. Lee, "Quantitative biosensing based on a liquid crystal marginally aligned by the PVA/DMOAP composite for optical signal amplification," Biosensors **12**(4), 218 (2022).

13. H.-G. Lee, S. Munir, and S.-Y. Park, "Cholesteric liquid crystal droplets for biosensors," ACS Appl. Mater. Interfaces **8**(39), 26407–26417 (2016).

14. J. M. Brake, M. K. Daschner, Y.-Y. Luk, and N. L. Abbott, "Biomolecular interactions at phospholipid-decorated surfaces of liquid crystals," Science **302**(5653), 2094–2097 (2003).

15. D. K. Nguyen and C.-H. Jang, "A cationic surfactant-decorated liquid crystal-based aptasensor for label-free detection of malathion pesticides in environmental samples," Biosensors **11**(3), 92 (2021).

16. M. R. Foreman, J. D. Swaim, and F. Vollmer, "Whispering gallery mode sensors," Adv. Opt. Photonics **7**(2), 168–240 (2015).

17. N. Toropov, G. Cabello, M. P. Serrano, R. R. Gutha, M. Rafti, and F. Vollmer, "Review of biosensing with whispering-gallery mode lasers," Light: Sci. Appl. **10**(1), 42 (2021).

18. Y. Zhi, X.-C. Yu, Q. Gong, L. Yang, and Y.-F. Xiao, "Single nanoparticle detection using optical microcavities," Adv. Mater. **29**, 1604920 (2017).

19. R. Duan, X. Hao, Y. Li, and H. Li, "Detection of acetylcholinesterase and its inhibitors by liquid crystal biosensor based on whispering gallery mode," Sensors and Actuators B: Chemical **308**, 127672 (2020).

20. Z. Wang, Y. Liu, H. Wang, S. Wang, K. Liu, T. Xu, J. Jiang, Y.-C. Chen, and T. Liu, "Ultra-sensitive dnazyme-based optofluidic biosensor with liquid crystal-au nanoparticle hybrid amplification for molecular detection," Sensors and Actuators B: Chemical **359**, 131608 (2022).

21. H. Wan, J. Chen, C. Wan, Q. Zhou, J. Wang, and Z. Zhang, "Optofluidic microcapillary biosensor for label-free, low glucose concentration detection," Biomed. Opt. Express **10**(8), 3929–3937 (2019).

22. M. Humar, M. Ravnik, S. Pajk, and I. Muševič, "Electrically tunable liquid crystal optical microresonators," Nat. Photonics **3**(10), 595–600 (2009).

23. H. Li, B. Sun, Y. Yuan, and J. Yang, "Guanidine derivative polymer coated microbubble resonator for high sensitivity detection of co 2 gas concentration," Opt. Express **27**(3), 1991–2000 (2019).

24. R. Duan, Y. Li, H. Li, and J. Yang, "Detection of heavy metal ions using whispering gallery mode lasing in functionalized liquid crystal microdroplets," Biomed. Opt. Express **10**(12), 6073–6083 (2019).

25. Y.-N. Zhang, T. Zhou, B. Han, A. Zhang, and Y. Zhao, "Optical bio-chemical sensors based on whispering gallery mode resonators," Nanoscale **10**(29), 13832–13856 (2018).

26. Y. Wang, L. Zhao, A. Xu, L. Wang, L. Zhang, S. Liu, Y. Liu, and H. Li, "Detecting enzymatic reactions in penicillinase via liquid crystal microdroplet-based ph sensor," Sensors and Actuators B: Chemical **258**, 1090–1098 (2018).

27. C. Lam, P. T. Leung, and K. Young, "Explicit asymptotic formulas for the positions, widths, and strengths of resonances in mie scattering," J. Opt. Soc. Am. B **9**(9), 1585–1592 (1992).

28. Q. Lu, J. Liao, S. Liu, X. Wu, L. Liu, and L. Xu, "Precise measurement of micro bubble resonator thickness by internal aerostatic pressure sensing," Opt. Express **24**(18), 20855–20861 (2016).

29. J. Jiang, Y. Liu, K. Liu, S. Wang, Z. Ma, Y. Zhang, P. Niu, L. Shen, and T. Liu, "Wall-thickness-controlled microbubble fabrication for wgm-based application," Appl. Opt. **59**(16), 5052–5057 (2020).

30. C.-Y. Xue and K.-L. Yang, "Dark-to-bright optical responses of liquid crystals supported on solid surfaces decorated with proteins," Langmuir **24**(2), 563–567 (2008).

31. E. P. Diamandis and T. K. Christopoulos, "The biotin-(strept) avidin system: principles and applications in biotechnology," Clin. chemistry **37**(5), 625–636 (1991).

32. M. Khan and S.-Y. Park, "Specific detection of avidin–biotin binding using liquid crystal droplets," Colloids and Surfaces B: Biointerfaces **127**, 241–246 (2015).

33. Q. Wang, S. Liu, L. Liu, and L. Xu, "Optomechanics in anisotropic liquid crystal-filled micro-bubble resonators," Opt. Express **27**(12), 17051–17060 (2019).
34. S. Arnold, M. Khoshsima, I. Teraoka, S. Holler, and F. Vollmer, "Shift of whispering-gallery modes in microspheres by protein adsorption," Opt. Lett. **28**(4), 272–274 (2003).
35. L. Bi, J. Dong, W. Xie, W. Lu, W. Tong, L. Tao, and W. Qian, "Bimetallic gold–silver nanoplate array as a highly active sers substrate for detection of streptavidin/biotin assemblies," Anal. chimica acta **805**, 95–100 (2013).
36. Q. Wang, X. Huang, X. Fu, H. Deng, M. Ma, and Z. Cai, "A sensitive and selective resonance rayleigh scattering method for quick detection of avidin using affinity labeling au nanoparticles," Spectrochimica Acta Part A: Mol. Biomol. Spectrosc. **162**, 75–80 (2016).